Supplement of Geosci. Instrum. Method. Data Syst., 12, 239–257, 2023
https://doi.org/10.5194/gi-12-239-2023-supplement

Geoscientific Instrumentation Methods and Data Systems
Open Access
EGU

Supplement of

Daedalus Ionospheric Profile Continuation (DIPCont): Monte Carlo studies assessing the quality of in situ measurement extrapolation

Joachim Vogt et al.

Correspondence to: Joachim Vogt (jvogt@constructor.university)

Supplementary Figures S1a–S1d

The four diagrams show profiles of atmospheric density and temperature parameters computed from output of the empirical atmospheric model NRLMSIS 2.0 for 12:00 UT, geographic longitude $0°$, and three latitudes: $\beta = 15°$ (first row), $\beta = 45°$ (second row), $\beta = 75°$ (third row). Simulation results have been provided by the Community Coordinated Modeling Center at Goddard Space Flight Center through their publicly available simulation services (https://ccmc.gsfc.nasa.gov). The empirical atmospheric model NRLMSIS 2.0 was developed by John Emmert and Douglas Drob at NRL. For further information, see

> Emmert, J. T., Drob, D. P., Picone, J. M., Siskind, D. E., Jones, M. Jr., Mlynczak, M. G., et al. (2020). *NRLMSIS 2.0: A whole-atmosphere empirical model of temperature and neutral species densities.* Earth and Space Science, 7, e2020EA001321. https://doi.org/ 10.1029/2020EA001321

The first column displays the total mass density together with partial mass densities of N_2, O_2, O, and Ar. The second column shows the average neutral molar mass $\langle M_n \rangle$ in units of g/mol as given by $\langle M_n \rangle = \sum_s M_{n,s} N_{n,s} / \sum_s N_{n,s}$, where $M_{n,s}$ is the molar mass of species s. The corresponding number densities $N_{n,s}$ are provided by the NRLMSIS 2.0 model, as well as the neutral temperature profile shown in the third column. In the fourth column, the resulting profle of pressure scale height is shown. The fifth column displays the relative change of neutral temperature and of average neutral molar mass. Each diagram represent one of the four seasons in the year 2018: Figure S1a – Spring equinox, 20 March 2018; Figure S1b – Summer solstice, 21 June 2018; Figure S1c – Autumn equinox, 23 September 2018; Figure S1d – Winter solstice, 21 December 2018.

Figure S1a (Spring equinox, 20 March 2018, 12:00 UT, geographic longitude 0°)

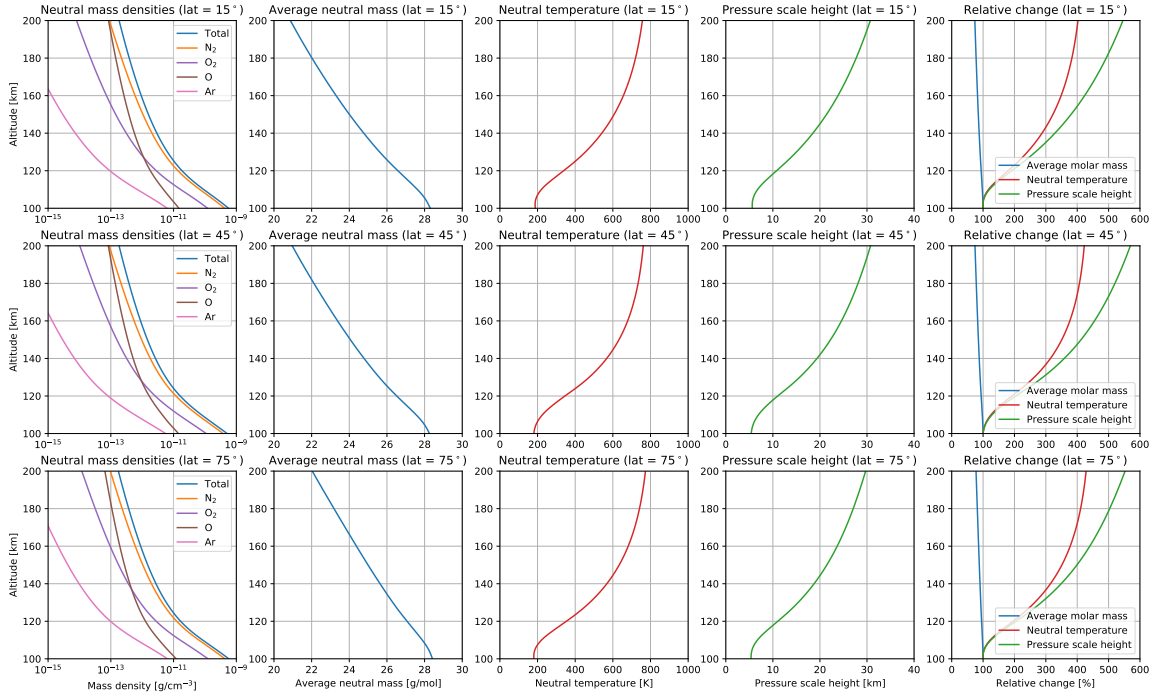

Figure S1b (Summer solstice, 21 June 2018, 12:00 UT, geographic longitude 0°)

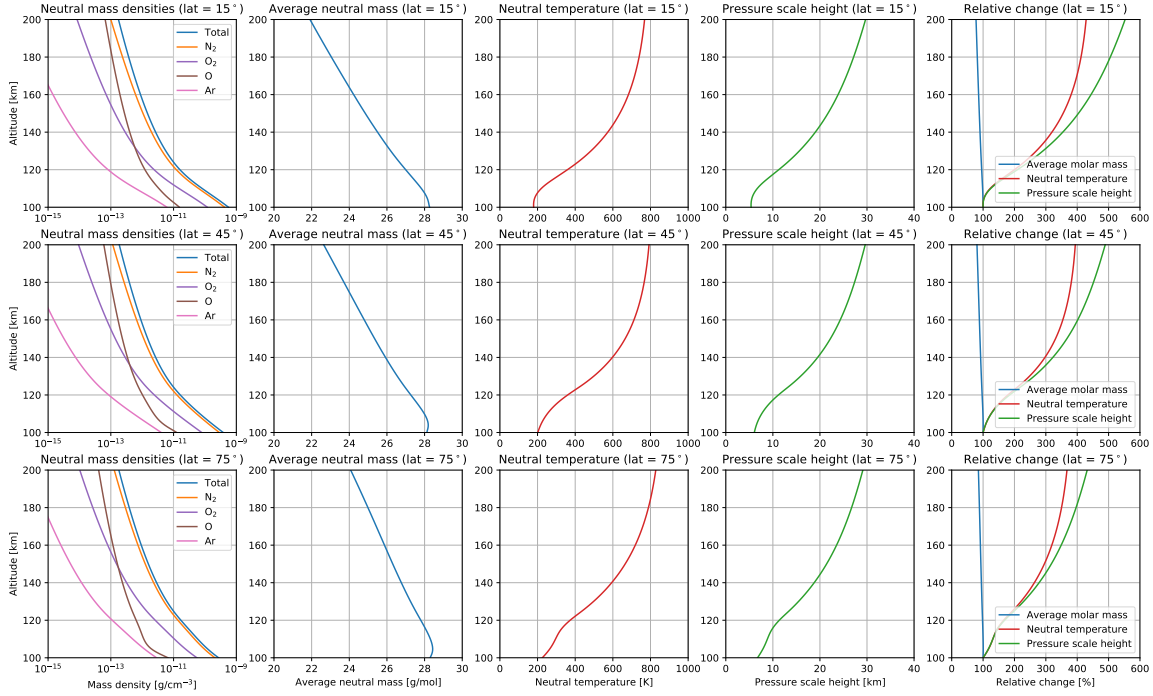

20

Figure S1c (Autumn equinox, 23 September 2018, 12:00 UT, geographic longitude 0°)

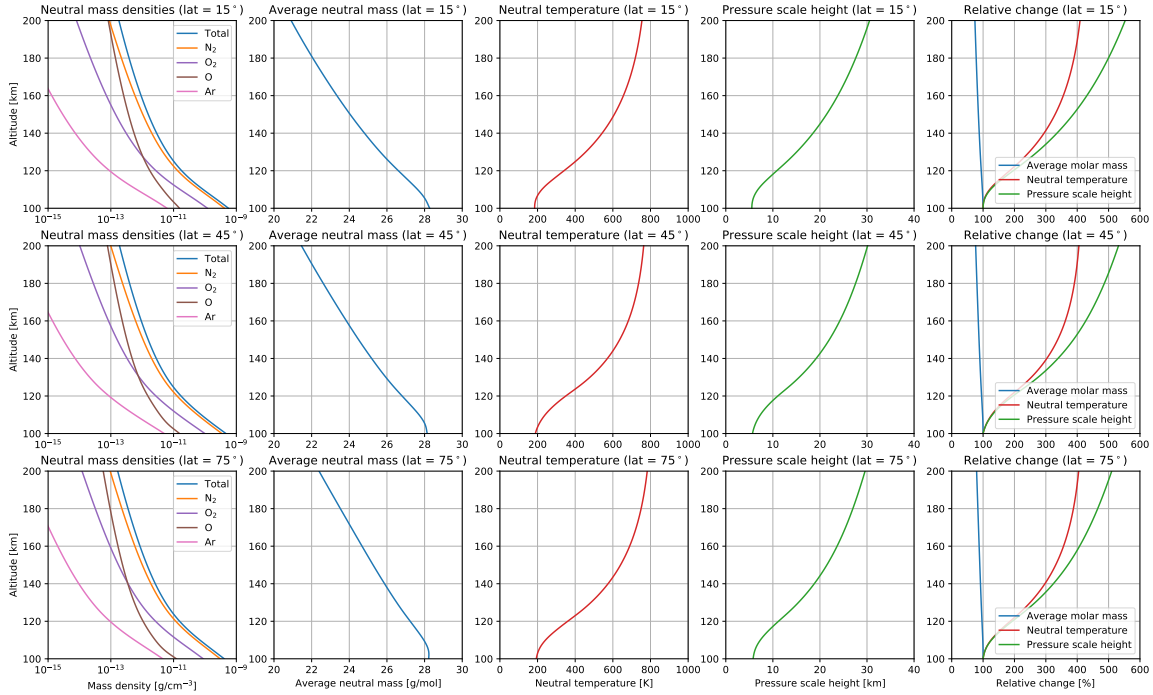

Figure S1d (Winter solstice, 21 December 2018, 12:00 UT, geographic longitude 0°)

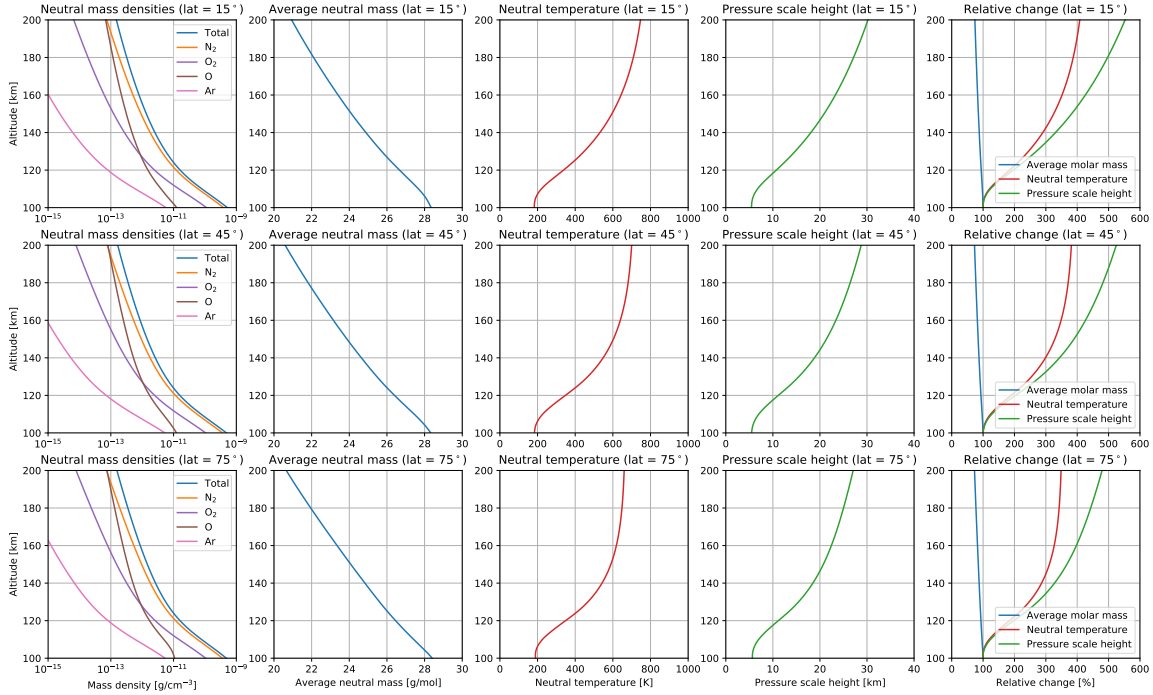

Supplementary Figures S2a–S2d

The four diagrams show profiles of ionospheric parameters computed from output of the Ionospheric Reference Ionosphere (IRI) 2020 model for 12:00 UT, geographic longitude $0°$, and three latitudes: $\beta = 15°$ (first row), $\beta = 45°$ (second row), $\beta = 75°$ (third row). Simulation results have been provided by the Community Coordinated Modeling Center at Goddard Space Flight Center through their publicly available simulation services (https://ccmc.gsfc.nasa.gov). The International Reference Ionosphere (IRI) 2020 Model was developed by the URSI/COSPAR Working Group on IRI. For further information, see

> Bilitza, D., Pezzopane, M., Truhlik, V., Altadill, D., Reinisch, B. W., Pignalberi, A. (2022). *The International Reference Ionosphere model: A review and description of an ionospheric benchmark.* Reviews of Geophysics, 60, e2022RG000792. https://doi. org/10.1029/2022RG000792

The first column displays the percentages P_s of the three main contributor species s to ion density in the region below 200 km, namely, NO^+, O_2^+, and O^+ ions. The second column shows the average ion molar mass $\langle M_i \rangle$ in units of g/mol as given by $\langle M_i \rangle = \sum_s M_{i,s} P_s / \sum_s P^s$, where $M_{i,s}$ is the molar mass of species s. Profiles of neutral temperature T_n, ion temperature T_i, and electron temperature T_e are shown in the third column. Note that a dashed linestyle was chosen for the T_i profile to show that in the range between 100 km and 200 km, it coincides with the T_n profile. Each diagram represent one of the four seasons in the year 2018: Figure S2a – Spring equinox, 20 March 2018; Figure S2b – Summer solstice, 21 June 2018; Figure S2c – Autumn equinox, 23 September 2018; Figure S2d – Winter solstice, 21 December 2018.

Figure S2a (Spring equinox, 20 March 2018, 12:00 UT, geographic longitude 0°)

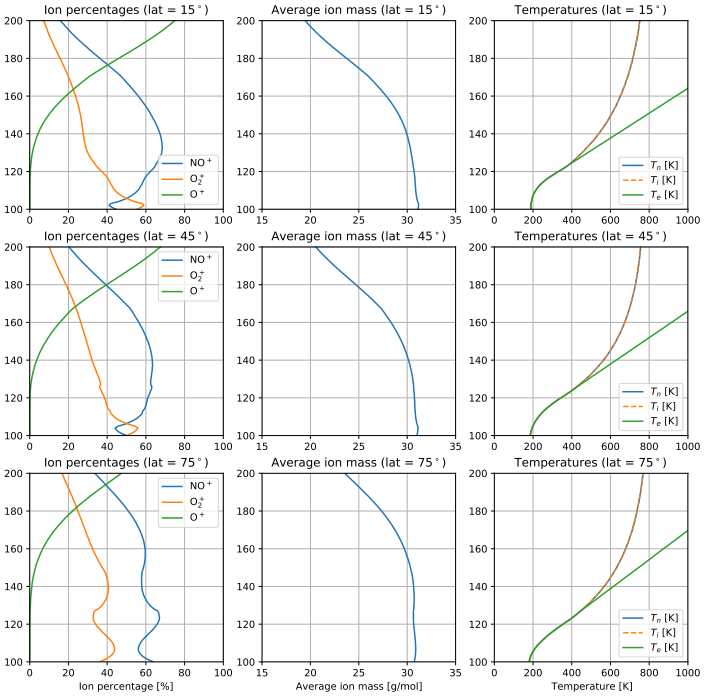

Figure S2b (Summer solstice, 21 June 2018, 12:00 UT, geographic longitude 0°)

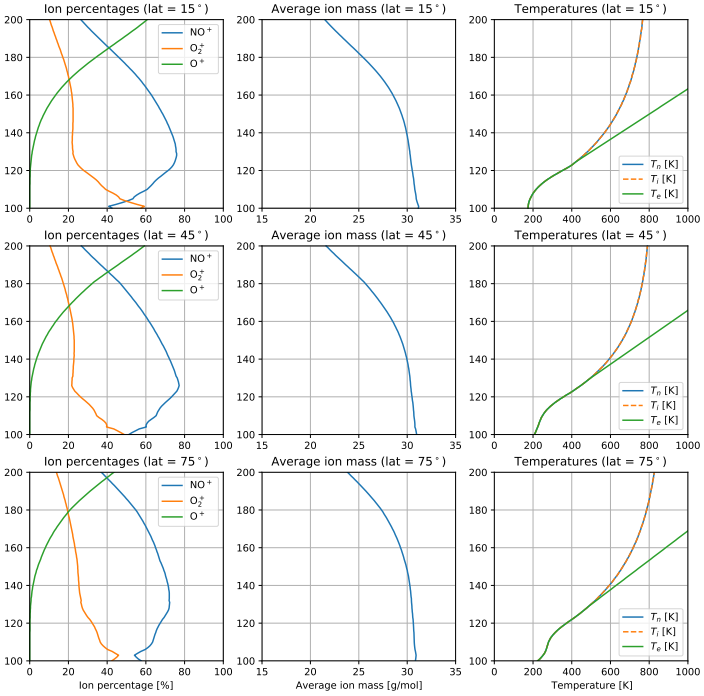

Figure S2c (Autumn equinox, 23 September 2018, 12:00 UT, geographic longitude 0°)

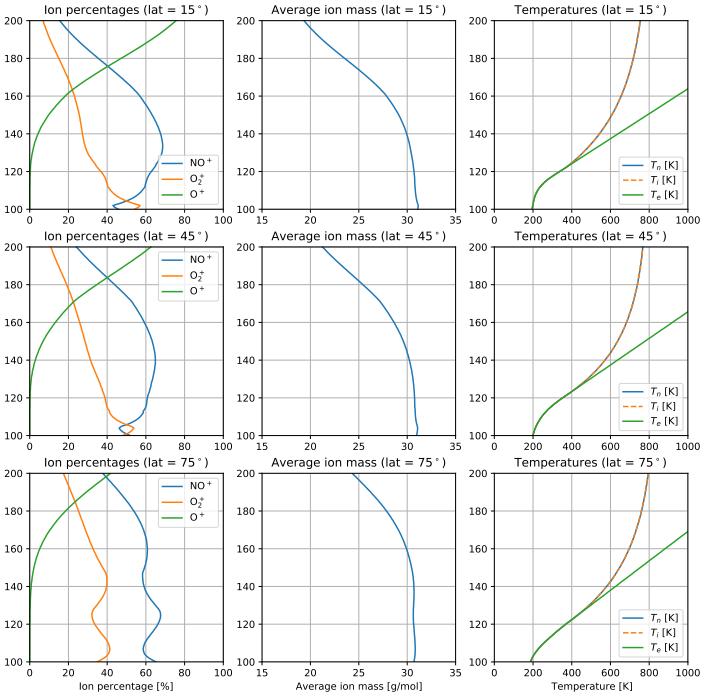

Figure S2d (Winter solstice, 21 December 2018, 12:00 UT, geographic longitude 0°)

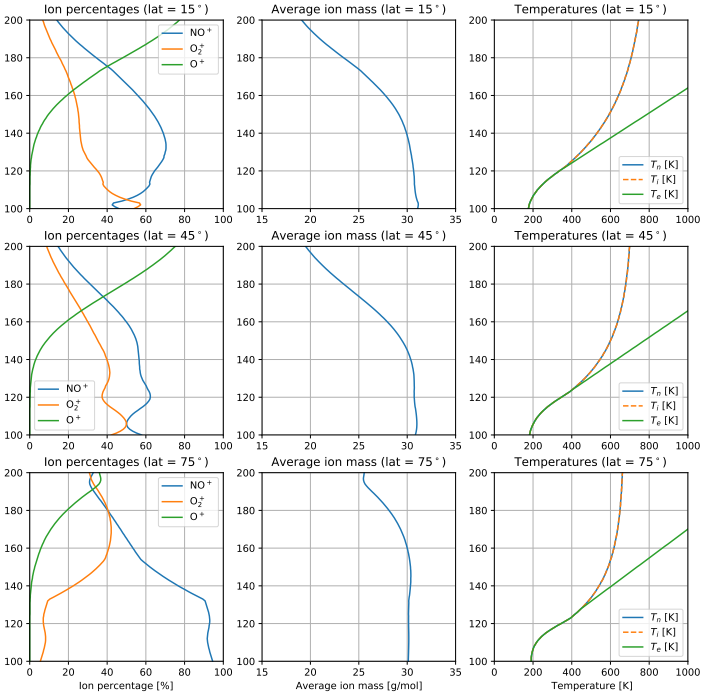

Supplementary Figure S3

The graphics provides additional information on the DIPCont modeling results shown in Figures 4, 5, 6. Variables displayed in Figure S3: neutral temperature (first row), neutral density (second row), electron density (third row), ion temperature (fourth row), ion-neutral collision frequency (fifth row), Pederson conductivity (sixth row).

First column: Model distributions of LTI variables. Synthetic measurements are produced along the two satellite orbits (white dashed lines). The parameters of vertical profiles are estimated using measurements within a window (white solid rectangle) around two locations in horizontal direction (blue and green dashed lines).

Second column and fourth column: Visualization of the ensemble of altitude profiles generated from the Monte Carlo distributions of model parameters. Shown are selected quantiles evaluated at the vertical grid of LTI altitudes. Second column: center position (blue dashed line) indicated in the first column diagram. Fourth column: right position (green dashed line) indicated in the first column diagram.

Third column and fifth column: Solid lines (blue and green) give the relative root-mean-square deviations of Monte Carlo altitude profiles from the respective input model profiles. Vertical dotted and solid lines represent a set of chosen error levels, ranging from 0.5 % and 1 % (yellow) to 32% and 64% (magenta). The corresponding horizontal lines show the extrapolation horizons indicating at which altitude the relative deviation equals the respective error level. Third column: center position (blue dashed line) indicated in the first column diagram. Fifth column: right position (green dashed line) indicated in the first column diagram.

Figure S3

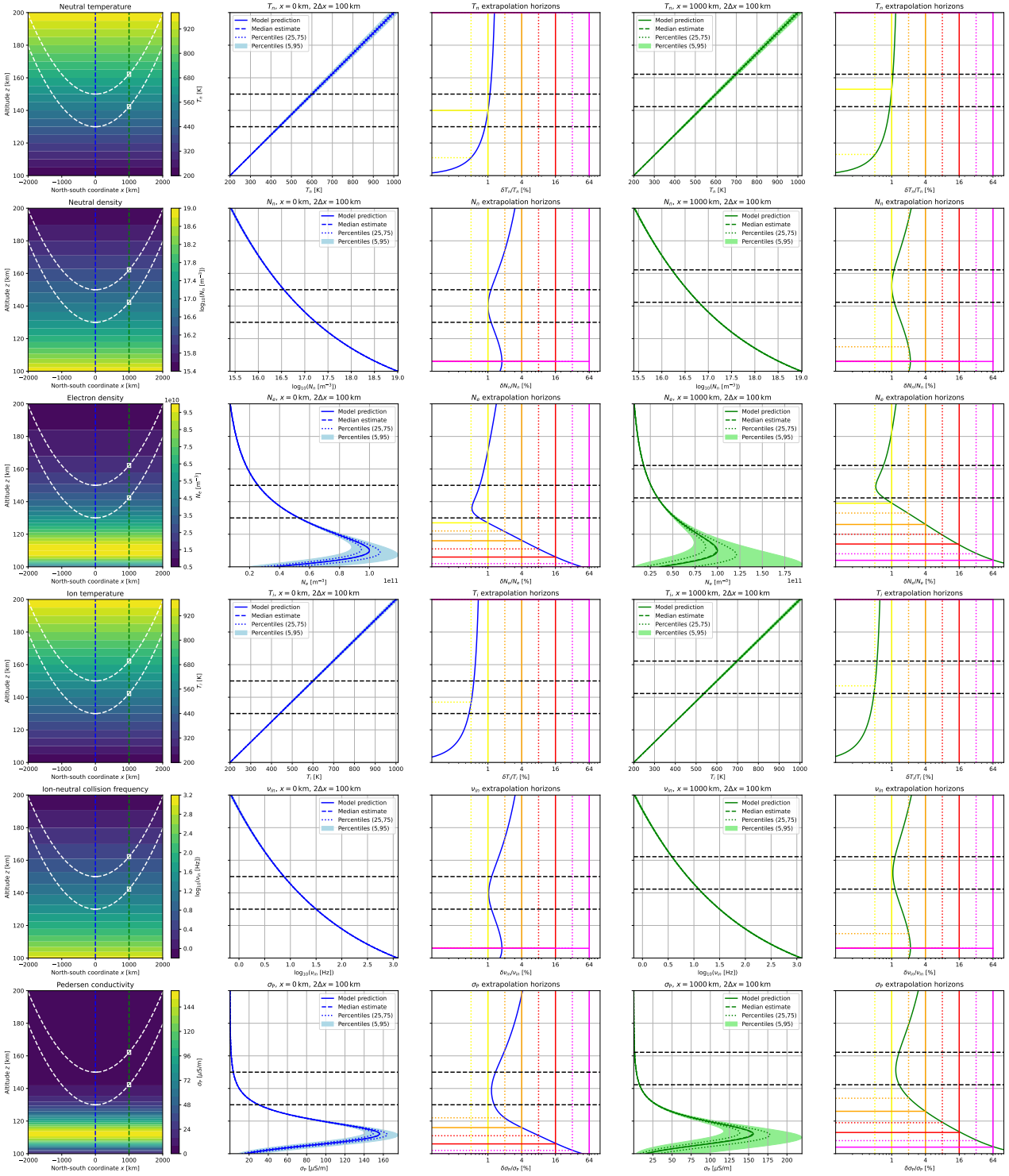
Neutral temperature
Neutral density
Electron density
Ion temperature
Ion-neutral collision frequency
Pedersen conductivity
Altitude z [km]
North-south coordinate x [km]
Model prediction
Median estimate
Percentiles (25,75)
Percentiles (5,95)

Supplementary Figure S4a

The diagram illustrates how visit times of ground horizontal distances are expected to differ for the two satellites of a dual-spacecraft mission to the LTI, provided they share the same orbital plane, have identical semi-major axes, and pass through their perigees at the same time. In the example, satellite A is on a Keplerian orbit with perigee altitude $z^A_{\rm per} = 130\,{\rm km}$ and apogee altitude $z^A_{\rm apo} = 3000\,{\rm km}$. Perigee and apogee altitudes of satellite B are $z^B_{\rm per} = 150\,{\rm km}$ and $z^B_{\rm apo} = 2980\,{\rm km}$, respectively. The orbits are computed using Stoermer-Verlet integration of the equation of motion. Left panel: Satellite altitudes z versus ground horizontal distance x. Center panel: Satellite visit times $t^A = t^A(x)$ and $t^B = t^B(x)$ at ground horizontal distance x. Right panel: Difference $\Delta t(x) = t^B(x) - t^A(x)$ of satellite visit times at ground horizontal distance x.

Supplementary Figure S4b

The diagram provides additional information on the satellite orbit representations implemented in the DIPCont package, using a satellite on a Keplerian orbit with perigee altitude $z_{\rm per} = 130\,{\rm km}$ and apogee altitude $z_{\rm apo} = 3000\,{\rm km}$ as an example. Compared are the results of Stoermer-Verlet integration and the local polynomial approximation constructed in the Appendix of the manuscript. Time and ground horizontal distance are centered at the perigee location. Upper left panel: Altitude z versus time t. Lower left panel: Ground horizontal distance x versus time t. Upper right panel: Altitude deviation of the local polynomial approximation relative to the result of the Stoermer-Verlet integration. Lower right panel: Ground horizontal distance deviation of the local polynomial approximation relative to the result of the Stoermer-Verlet integration.

Figure S4a

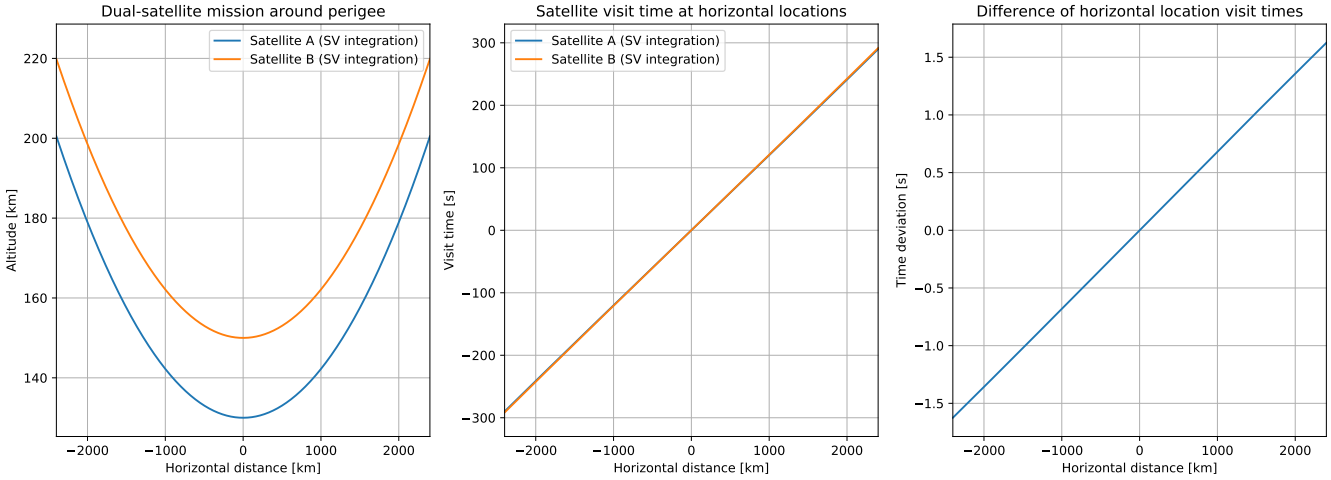

Figure S4b